


Cerebral hypomyelination associated with biallelic variants of *FIG4*

Guy M. Lenk¹  | Ian R. Berry² | Chloe A. Stutterd^{3,4,5} | Moira Blyth⁶ | Lydia Green⁷ | Gayatri Vadlamani⁷ | Daniel Warren⁸ | Ian Craven⁸ | Miriam Fanjul-Fernandez^{3,4} | Victoria Rodriguez-Casero⁵ | Paul J. Lockhart^{3,4} | Adeline Vanderver⁹ | Cas Simons^{3,10} | Susan Gibb^{4,5} | Simon Sadedin^{3,4} | Broad Center for Mendelian Genomics | Susan M. White^{3,4,11} | John Christodoulou^{3,4,11} | Olga Skibina¹² | Jonathan Ruddle^{5,13,14} | Tiong Y. Tan^{3,4,11} | Richard J. Leventer^{3,4,5} | John H. Livingston⁷ | Miriam H. Meisler¹

¹Department of Human Genetics, University of Michigan, Ann Arbor, Michigan

²Leeds Genetics Laboratory, The Leeds Teaching Hospitals NHS Trust, St James's University Hospital, Leeds, UK

³Murdoch Children's Research Institute, Melbourne, Australia

⁴Department of Paediatrics, University of Melbourne, Melbourne, Australia

⁵Royal Children's Hospital, Melbourne, Australia

⁶Yorkshire Regional Genetics Service, The Leeds Teaching Hospitals NHS Trust, Chapel Allerton Hospital, Leeds, UK

⁷Paediatric Neurology, The Leeds Teaching Hospitals NHS Trust, Leeds General Infirmary, Leeds, UK

⁸The Leeds Teaching Hospitals NHS Trust, Leeds General Infirmary, Leeds, UK

⁹Division of Neurology, Children's Hospital of Philadelphia and Perelman School of Medicine, University of Pennsylvania, Philadelphia, Pennsylvania

¹⁰Institute for Molecular Bioscience, University of Queensland, St Lucia, Australia

¹¹Victorian Clinical Genetics Services, Melbourne, Australia

¹²Eastern Health Neurosciences, Box Hill Hospital, Monash University, Melbourne, Australia

¹³Centre for Eye Research Australia Ltd, East Melbourne, Victoria, Australia

¹⁴Department of Ophthalmology, University of Melbourne, Melbourne, Australia

Correspondence

Miriam H. Meisler, University of Michigan, Department of Human Genetics, 1241 East Catherine, 4909 Buhl, Ann Arbor, MI 48109-0618.
Email: meislerm@umich.edu

Funding information

National Institute of General Medical Sciences, Grant/Award Number: R01 GM24872; National Human Genome Research Institute, National Eye Institute, and National Heart, Lung and Blood Institute, Grant/Award Number: UM1 HG008900; NHMRC Postgraduate Scholarship, Grant/Award Number: GNT1133266; Neurogenetics Fellowship from Thyne-Reid Foundation and Macquarie Foundation; NHMRC Independent Research Institute Infrastructure Support Scheme; Victorian State Government Operational Infrastructure Program

Abstract

The lipid phosphatase gene *FIG4* is responsible for Yunis-Varón syndrome and Charcot-Marie-Tooth disease Type 4J, a peripheral neuropathy. We now describe four families with *FIG4* variants and prominent abnormalities of central nervous system (CNS) white matter (leukoencephalopathy), with onset in early childhood, ranging from severe hypomyelination to mild undermyelination, in addition to peripheral neuropathy. Affected individuals inherited biallelic *FIG4* variants from heterozygous parents. Cultured fibroblasts exhibit enlarged vacuoles characteristic of *FIG4* dysfunction. Two unrelated families segregate the same G > A variant in the +1 position of intron 21 in the homozygous state in one family and compound heterozygous in the other. This mutation in the splice donor site of exon 21 results in read-through from exon 20 into intron 20 and truncation of the final 115 C-terminal amino acids of *FIG4*, with retention of partial function. The observed CNS white matter disorder in these families is consistent with the myelination defects

in the FIG4 null mouse and the known role of FIG4 in oligodendrocyte maturation. The families described here the expanded clinical spectrum of FIG4 deficiency to include leukoencephalopathy.

KEYWORDS

CMT4J, dysmyelination, endolysosome, leukodystrophy, neurodegeneration, oligodendrocyte, PIKFYVE, VAC14, vacuolization, PtdIns(3,5)P₂

1 | INTRODUCTION

Neurological effects of *FIG4* mutations were first described in a mouse mutant with a loss-of-function mutation that resulted in neuronal degeneration, dysmyelination in the central nervous system (CNS) and the peripheral nervous system (PNS), and juvenile lethality (Chow et al., 2007; Mironova et al., 2016; Winters et al., 2011). The corresponding human disorder with homozygous loss-of-function of *FIG4* is the Yunis-Varón syndrome, a multi-system disorder with severe neurological and skeletal defects, CNS dysmyelination, and juvenile lethality (Campeau et al., 2013). Partial loss-of-function of *FIG4* can result in Charcot-Marie-Tooth disease (CMT) Type 4J, an autosomal recessive peripheral neuropathy with myelin defects restricted to the PNS (Chow et al., 2007; Nicholson et al., 2011). In one consanguineous family, a homozygous missense variant of *FIG4* results in polymicrogyria and psychiatric features, but no CNS demyelination (Baulac et al., 2014). Therefore, to date, impaired CNS myelination has been associated with complete loss-of-function of *FIG4* in Yunis-Varón syndrome, but not with partial loss-of-function because of missense variants.

The FIG4 protein is a subunit of the PI(3,5)P₂ biosynthetic complex that also contains PIKFYVE, a PI3P kinase, and VAC14, a scaffold protein. Recessive variants of *VAC14* in human and mouse mimic the clinical and cellular defects of *FIG4* deficiency (Jin et al., 2008; Lenk et al., 2016b; Stutterd et al., 2017). Variants that reduce *VAC14* abundance also destabilize the FIG4 protein (Lenk et al., 2011; Zolov et al., 2012). The product of the biosynthetic complex, PI(3,5)P₂, is a low abundance signaling lipid that activates ion channels in the lysosomal membrane, including TRPML1, TPC1, and TPC2 (Dong et al., 2010; Kirsch, Kugemann, Carpaneto, Böckmann, & Dietrich, 2018; She et al., 2018; Wang et al., 2012; Wilson, Scott, Dowell, & Odorizzi, 2018). At the cellular level, low levels of PI(3,5)P₂ lead to accumulation of large and acidic lysosome-derived vesicles (Chow et al., 2007; Ferguson et al., 2012; Ferguson, Lenk, & Meisler, 2009). These enlarged vesicles appear to be resulting from osmotic swelling of lysosomes secondary to deficient activation of ion channels in the lysosome membrane (Lenk & Meisler, 2014). FIG4 deficiency may be considered one of the lysosomal disorders affecting lysosomal membrane function rather than enzymatic degradation of macromolecules (McDonald & Krainc, 2017).

A direct role of FIG4 in CNS myelination is indicated by defective oligodendrocyte maturation and myelin biosynthesis in *FIG4* null mice (Mironova et al., 2016). In addition, targeted inactivation of

FIG4 in Schwann cells causes peripheral nerve demyelination, demonstrating a role in the PNS (Vaccari et al., 2015).

In this report, we describe patients with rare variants of *FIG4* in whom abnormalities of CNS white matter is a predominant feature. In view of these observations, we suggest that *FIG4* should be considered a candidate gene in individuals presenting with primary defects in CNS white matter.

2 | METHODS

2.1 | DNA sequencing

Families 1 and 2 were consented for clinical exome sequencing as part of their formal diagnostic work-up at Leeds Teaching Hospitals NHS Trust. Sequencing was performed using the Agilent SureSelectXT Focused Exome reagent (Agilent Technologies, Wokingham, UK) and sequenced on an Illumina HiSeq. 2500 rapid mode flow cell (Illumina Inc., San Diego, CA) with 2 × 101 nt paired-end reads for Family 1, and an Illumina NextSeq. 500 with 2 × 151 nt paired-end reads for Family 2. A custom bioinformatics pipeline was applied, comprising Cutadapt v.1.9.1 for the adaptor and quality trimming, BWA-mem for read alignment, GATK UnifiedGenotyper for variant calling, Alamut batch v.1.4.0 for variant annotation, and the GATK walkers DepthOfCoverage, CallableLoci and CountReads for generating coverage data. The analysis was restricted initially to a list of 98 genes known to be associated with white matter conditions, and then expanded to a manually-curated list of 2,060 genes associated with or candidates for human developmental and neuromuscular diseases. Identified *FIG4* variants were also analyzed by bidirectional Sanger sequencing in probands and parents.

Family 3 consented to participate in a gene discovery project approved by the Royal Children's Hospital Human Research Ethics Committee (HREC number 28097). Whole genome sequencing was performed for both affected individuals and both parents using 2 × 150 nt paired-end reads on an Illumina X (Illumina Cambridge Ltd, Little Chesterford, UK). Read alignment was performed using BWA-mem; the variant calling of the nuclear genome was performed using GATK HaplotypeCaller v3.7, BCFtools was used to call mtDNA variants. (Li & Durbin, 2009, McKenna et al., 2010) SnpEff v4.3m was used for variant annotation and a custom script was utilized for variant filtration and prioritization. (Cingolani et al., 2012). No additional relevant variants were observed in Family 3.

Family 4 underwent exome sequencing at the Center for Mendelian Genomics at the Broad Institute after written informed consent to participate in the Murdoch Children's Research Institute Undiagnosed Diseases Project (RCH HREC 36291A).

2.2 | Cell culture

Patient cells were grown in RPMI 1640 medium supplemented with 15% fetal bovine serum and 1% Antibiotic-Antimycotic solution (Gibco) on vacuum gas plasma treated dishes (Corning) at 37°C with 5% CO₂ supplementation. Vacuolization was assessed as previously described (Lenk et al., 2016a). Briefly, cells were plated at 20,000 cells/cm² for 18 hr before assessment of vacuolation. Cells were imaged without selection and scored as described.

3 | RESULTS

3.1 | Clinical features of affected children in four families with *FIG4* variants

The clinical features of the affected individuals are described below and summarized in Table 1. Family 1: Patient 1 is currently 4 years of age. He presented at 6 months with developmental delay and hypotonia. His initially rapid head growth stabilized at the 75th centile by the age of two. He began sitting without support at 12 months and has made slow developmental progress, but at the age of 4 years he is not able to walk without support. He has generalized hypotonia with absent deep tendon reflexes. His brain magnetic resonance imaging (MRI) showed a complete lack of cerebral myelination at 10 months and 27 months of age, as well as ventriculomegaly without cerebrospinal fluid obstruction. (Figure 1a–d). His progressive peripheral neuropathy is similar to patients with CMT4J, but the CNS deficits are distinct.

Family 2: Patient 2 is the first child of consanguineous South Asian parents. He was born at term and had initial feeding difficulties and severe motor delay with hypotonia and weakness. At 11 years of age, he is nonambulant and has profound generalized weakness. He is nonverbal but able to indicate his needs and identify favorite objects. After a chest infection, he required a tracheostomy and is fed by gastrostomy. Vision and hearing are normal. Nerve conduction studies demonstrate a severe motor and sensory demyelinating neuropathy. None of the skeletal features seen in Yunis-Varón syndrome were observed. Brain MRIs demonstrate abnormal signal in the internal capsule and cerebral white matter, which remained stable between 30 months and 8 years of age. There is a mild progressive volume loss of the cerebellar hemispheres (Figure 1e–h).

Family 3: The two affected siblings in Family 3 are currently aged 11 years (Patient 3) and 4 years (Patient 4) and experienced onset of symptoms at 9 months and 12 months, respectively. Patient 3 presented with profound hypotonia, developmental delay, and areflexia with disease progression that includes scoliosis. Patient 4 presented with a mild degree of gross motor and developmental

delay, depressed tendon reflexes and relative macrocephaly, and later developed strabismus. Both children have cognitive impairment, Patient 3 has low to borderline IQ and Patient 4 is nonverbal at 4 years of age. Nerve conduction studies in both siblings demonstrated lack of sensory responses and mild slowing of motor responses consistent with mild to moderate demyelinating peripheral neuropathy. Brain MRIs of both children demonstrate T2 hyperintensity in the cerebral white matter consistent with hypomyelination (Figure 1i–l). Patient 3 exhibited T2 hyperintensities without enhancement in the spinal cord and abnormal enhancement of cervical root and cauda equine suggestive of polyneuropathy (not shown). Patient 4 did not have spinal cord involvement.

X-rays demonstrate severe scoliosis and thin shafts of the tubular bones with over tubulation (Patient 3), delayed bone age (Patient 4) and thin metacarpals, coxa valga, and dolicocephaly in both siblings (Figure S1).

Family 4: Three affected siblings born to unrelated parents in Family 4 (Patients 5, 6, and 7) have a novel phenotype of severe global developmental delay, autistic features, and maculopathy. The proband (Patient 5) was first noted to have plagiocephaly, delayed milestones, abnormal tone, and choreoathetoid movements in infancy. The involuntary movements improved spontaneously by the age of 22 months. He also experienced gastroesophageal reflux with frequent vomiting that improved by 15 months of age with medical therapy and thickened feeds. At 11 years, he has limited communication and is incontinent. He has had no developmental regression. His brain imaging at 3 years of age demonstrated mild T2 hyperintensity of the periventricular white matter and mild ventricular dilatation (Figure 1m,n). Follow-up imaging demonstrated persistently delayed myelination, mild-moderate ventricular dilatation, reduction in white matter bulk, and mildly increased T2 and FLAIR signal within the deep white matter around the posterior bodies of the lateral ventricles. His male and female siblings exhibited a similar clinical course with delayed milestones and autistic features but without abnormal movements.

The ocular findings in each affected child in Family 4 were initially described as bull's eye maculopathy (Figure S2a,b). Preferential Cardiff acuity testing suggested a vision of 6/12 equivalent. There was a normal ocular movement, healthy ocular media, and no strabismus. The more severely affected sibling (Patient 6) also has optic atrophy, retinal atrophy, and vascular attenuation (Figure S2c,d). An optical coherence tomogram under anesthetic identified outer retinal atrophy, loss of foveal architecture, and generalized retinal thinning, including loss of the retinal nerve fiber layer with temporal optic disc pallor (Figure 2e,f).

The father was clinically unaffected, but the mother was diagnosed with multiple sclerosis at the age of 39, based on clinical presentation and MRI findings. She presented with progressive dizziness and ataxia of several weeks' duration. Review of her brain MRI demonstrated classical features of multiple sclerosis including widespread 2016a supra- and infratentorial demyelination, meeting the diagnostic criteria (Polman et al., 2011). Spinal cord imaging was normal. One episode of left arm numbness lasting for weeks occurred 7 years before

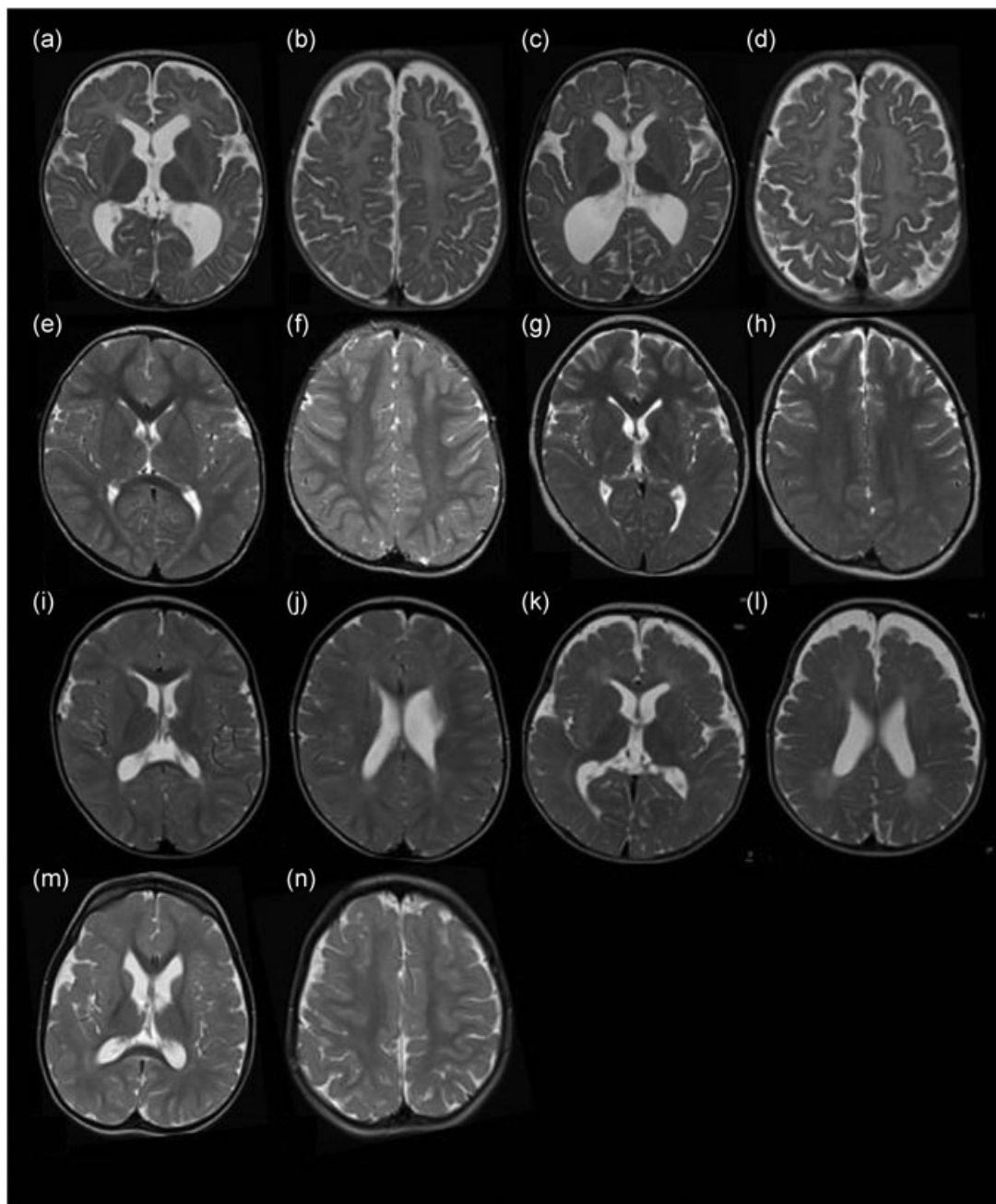


FIGURE 1 Evidence of CNS myelin defects in affected individuals carrying *FIG4* variants. MRI images. Axial T2 weighted MR images of patient 1 (Family 1) at 10 months (a,b) and 27 months (c,d) demonstrating the complete absence of myelination in cerebral white matter and internal capsule with no improvement on follow-up. Patient 2 (Family 2) at 30 months (e,f) and 8 years (g,h) demonstrates high signal in the posterior limb of the internal capsule and diffuse high signal in the posterior periventricular and deep cerebral white matter. Family 3, Sibling 1 at 25 months (i,j) demonstrates mild high signal in cerebral white matter with myelination present in deep and subcortical white matter. Family 3, Sibling 2 at 18 months (k,l) demonstrates more striking hypomyelination with very little normal myelin visible. The MRI of Patient 5 in Family 4 at 3 years of age was largely normal with nonspecific high signal in the periventricular and deep parietal white matter (m,n). CNS: central nervous system; MRI: magnetic resonance imaging

presentation, and there was fatigue during the last few years. Examination demonstrated truncal and right limb ataxia and subtle pyramidal deficit but no cognitive deficits. Ataxia improved after treatment with intravenous methylprednisolone. She was commenced on disease-modulating therapy with fingolimod soon after the diagnosis of multiple sclerosis and remains clinically stable.

3.2 | Identification and inheritance of *FIG4* mutations

Family 1: The affected individual is a compound heterozygote for the nonsense variant p.Trp246Ter (NM_014845.5: c.737G > C; (Allele 1) and a variant in the consensus + 1G nucleotide of the donor splice site of exon

21 (c.2459 + 1G > A; Allele 2; Figure 2a). Genotyping of the parents demonstrated that both variants were inherited (Figure 2a). In the gnomAD database (Lek et al., 2016), Allele 1 (rs776005417) is present in 10 heterozygotes and no homozygotes (allele frequency = 0.00005) and Allele 2, the splice site mutation (rs747768373), is present in four heterozygotes and no homozygotes (allele frequency = 0.000014).

Family 2: The affected individual is homozygous for the missense variant p.Tyr169Ser (c.506A > C). He is the first child of consanguineous South Asian parents. This ultra-rare missense variant is located in an evolutionarily conserved region of the protein and within six residues of the Yunis-Varón null mutation p.Leu175Pro (Campeau et al., 2013; Figure 2). This variant is present in three heterozygotes of South Asian origin in the gnomAD database and no homozygotes (allele frequency of 0.00001). Another substitution of this amino acid residue, p.Tyr169Cys, is found in gnomAD in seven heterozygotes and no homozygotes.

Family 3: Both affected individuals in Family 3 are homozygous for the exon 21 + 1 splice site mutation c.2459 + 1G > A (rs747768373) described above in Family 1. Both parents in Family 3 are of European non-Finnish origin. The four individuals in the gnomAD database who

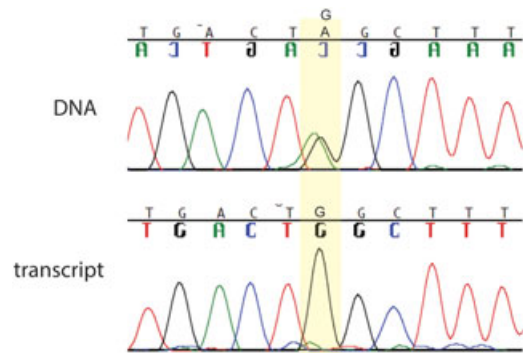


FIGURE 3 Nonsense-mediated decay of the Allele 1 transcript in Family 1. The affected individual is heterozygous for variant W246X in Exon 7. The sequence of the wildtype tryptophan codon TGG and the stop codon TAG are both evident in the PCR product from genomic DNA (top). In contrast, the product amplified by RT-PCR of fibroblast RNA contains the tryptophan codon TGG, but the stop codon is not detectable. The data demonstrates the instability of the stop-codon containing transcript, which is a predicted substrate for nonsense-mediated decay. RT-PCR: reverse transcription polymerase chain reaction [Color figure can be viewed at wileyonlinelibrary.com]

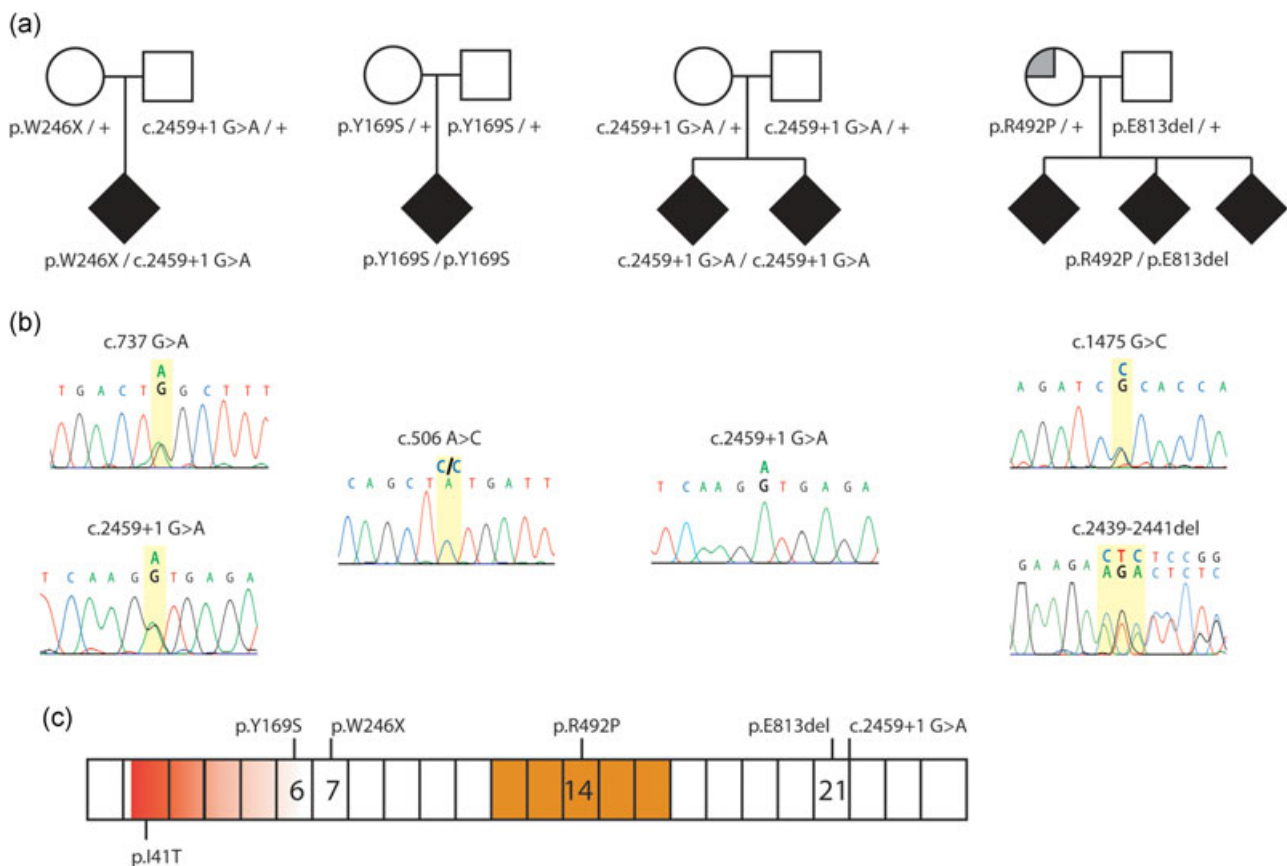


FIGURE 2 Recessive inheritance of *FIG4* variants in four families. (a) Affected individuals (solid symbols) are compound heterozygotes for inherited variants of *FIG4*. Carrier parents were unaffected (open symbols) except for the mother in Family 4 who was diagnosed with multiple sclerosis (partially filled symbol). (b) Genomic DNA sequences from affected individuals demonstrate two inherited mutant alleles. (c) Locations of variants on the *FIG4* protein. Exon borders are marked. Red, VAC14 protein interaction domain; gold, phosphatase catalytic active site. *FIG4* cDNA, NM_014845.5 [Color figure can be viewed at wileyonlinelibrary.com]

carry this variant are from European (non-Finnish) and African populations.

Family 4: The three affected siblings in Family 4 are compound heterozygotes for a maternally inherited in-frame deletion (c.2439_2441del; p.Glu813del) and a paternally inherited missense variant (c.1475G > C; p.Arg492Pro). The deletion of glutamate residue 813 changes the surrounding protein sequence from SerGluGluAsp to SerGluAsp. This deletion was observed in three out of 246,074 alleles in gnomAD but not in homozygous state (allele frequency 0.000012; Lek et al., 2016). The paternal allele is the novel missense variant p.Arg492Pro. Arginine 492 is an invariant residue located within the C(X)₅RT motif of the phosphatase active site. Substitution of this residue results in loss of phosphatase activity (Guan & Dixon, 1991; Liu & Bankaitis, 2010) and p.Arg492Pro is absent from the gnomAD database. Another substitution of this residue, p.Arg492Cys, is present in gnomAD in heterozygous state in two out of 246,238 alleles but not in homozygous state.

3.3 | Functional analysis of *FIG4* variants in patient fibroblasts and transfected cells

Cultured fibroblasts were obtained from affected individuals carrying the *FIG4* variants. Fibroblast RNA was analyzed to determine the effects of splice site and nonsense variants on transcript processing. Live-cell microscopy of fibroblast cultures was carried out to detect enlarged vacuoles characteristic of fibroblasts with deleterious variants of *FIG4*. These acidic vesicles are of lysosomal origin and LAMP1 and LAMP2 localize to their membranes (Lenk & Meisler, 2014).

Family 1: The transcript of Allele 1 with a stop codon in Exon 7 is a predicted substrate for nonsense-mediated decay. To evaluate the stability of the Allele 1 transcript, we compared the sequence of Exon 7 in genomic DNA and fibroblast RNA. Heterozygosity for the stop codon was detected by Sanger sequencing of the genomic PCR product, but only the wildtype sequence was present in the reverse transcription polymerase chain reaction (RT-PCR) product (Figure 3).

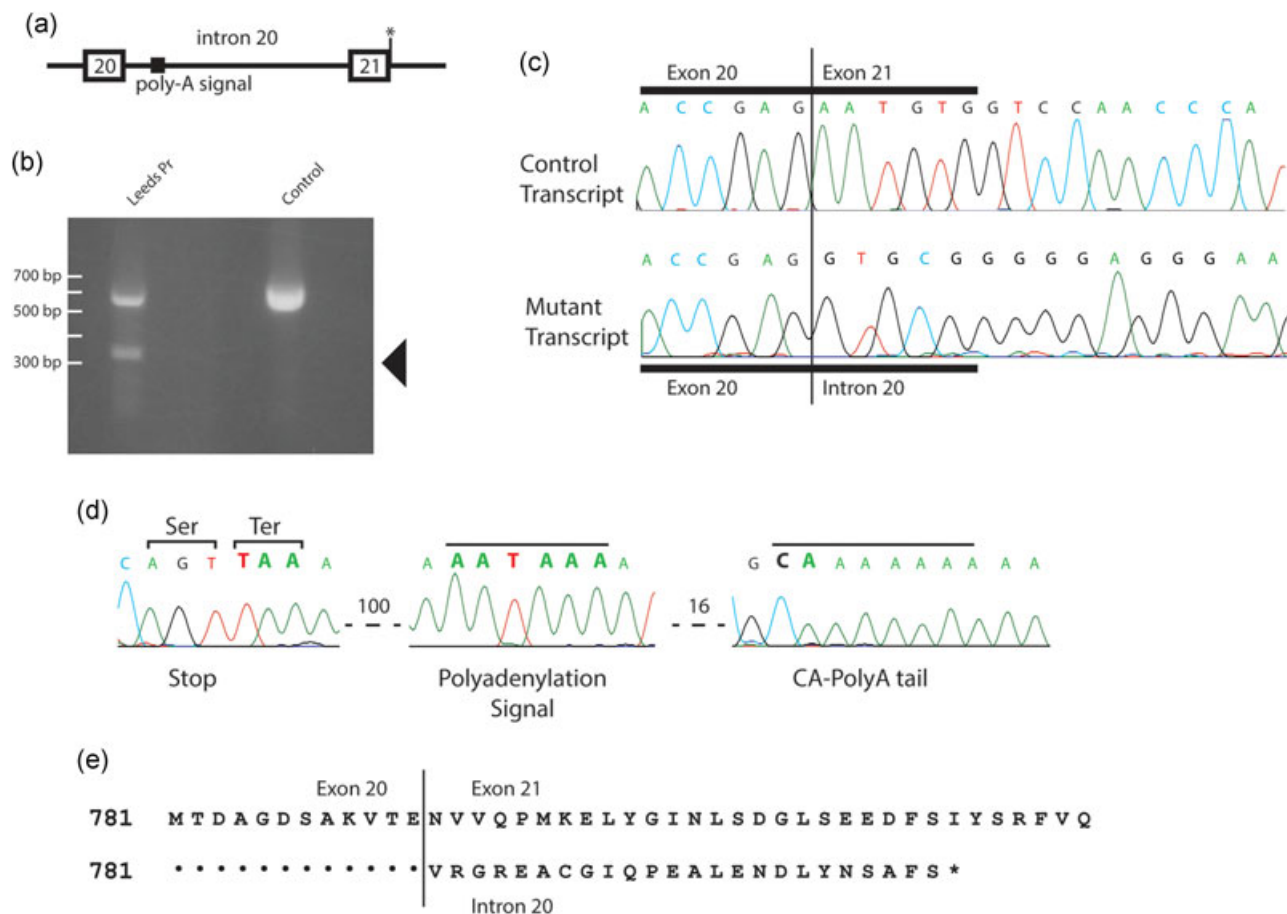


FIGURE 4 Retention of intron 20 in the allele 2 transcript in Family 1. (a) location of splice site mutation at exon 21 + 1 (asterisk). (b) Aberrant, short 3'-RACE product obtained using a forward primer in exon 20 on fibroblast RNA isolated from the affected individual in Family 1 (arrow). (c) Sanger sequence of purified 3'-RACE products demonstrates correct splicing from Exon 20 to Exon 21 in one transcript and readthrough from Exon 20 into Intron 20 in the other transcript. (d) Additional sequence of the aberrant, read-through 3'-RACE product demonstrates the use of the polyadenylation signal in Intron 20, 100 bp downstream from Exon 20. (e) The amino acid sequence of the truncated protein encoded by the read-through transcript [Color figure can be viewed at wileyonlinelibrary.com]

This result indicates that the transcript is subject to nonsense-mediated decay. The truncated protein that terminates at residue 246 is unlikely to be produced at significant levels, making this a null allele.

Allele 2 in Family 1 contains a G > A substitution at the +1 position of Intron 21 that is predicted to inactivate the splice donor site for Exon 21 (Figure 4a). Loss of the +1G nucleotide can lead either to skipping of the affected exon or to other alternative splicing. RT-PCR with a forward primer in Exon 20 and a reverse primer in exon 22 did not detect transcripts that skip exon 21. Therefore, to identify the aberrant transcript, we carried out 3'-RACE with a reverse oligo dT primer and a forward primer in Exon 20. Two products were obtained from heterozygous RNA, the predicted wildtype product containing Exons 20, 21, 22, and 23, and a shorter unique product of 325 bp (Figure 4b, arrow). Sequencing the gel-purified fragments demonstrated correct splicing from Exon 21–22 in the wildtype product, but read-through from Exon 20 into Intron 20 in the mutant 3'-RACE product (Figure 4c). The mutant product terminates at a cryptic polyadenylation signal beginning at position +176 in Intron 20 (Figure 4d). The mutant transcript encodes a predicted protein of 816 residues that terminates with 24 amino acids encoded by Intron 20 and lacks the 115 C-terminal residues of the wildtype protein.

Eighty percent of cultured patient fibroblasts contained enlarged vacuoles (Figure 5a,b) demonstrating that the truncated protein encoded by Allele 2 is not fully functional. The clinical features of the patient are much less severe than patients with Yunis-Varón syndrome, suggesting that the mutant protein does retain partial function. Patient 1 is thus heterozygous for one loss-of-function allele and one partial-loss-of-function allele.

Family 2: The affected individual is homozygous for the missense mutation p.Tyr169Ser. Tyr169 is located in a conserved region of the protein whose specific function is not known. Examination of cultured fibroblasts revealed the characteristic enlarged vacuoles described above for Patient 1, with a similar frequency of vacuolated cells (Figure 5a,b). p.Tyr169Ser thus appears to be a partial loss-of-function allele.

Family 3: The affected siblings in Family 3 are homozygous for the Exon 21 + 1 mutation characterized in Family 1 (Figure 3). The relatively mild phenotype of these children, compared to *FIG4* null individuals with Yunis-Varón syndrome is consistent with the evidence above that the C-terminal truncated protein retains partial activity.

Family 4: The three affected siblings in this family are compound heterozygotes for the amino acid deletion p.Glu813del (Allele 1) and the missense mutation p.Arg492Pro at the CX₅RT motif of the phosphatase active site. This invariant arginine residue stabilizes the dephosphorylation transition state and mutation of this residue results in loss of enzymatic activity in related enzymes (Guan & Dixon, 1991; Liu & Bankaitis, 2010). To determine whether allele 1 is deleterious, we examined cultured fibroblasts by light microscopy. The presence of enlarged vacuoles was evident (Figure 5). The fact that the affected individuals do not have Yunis-Varón syndrome

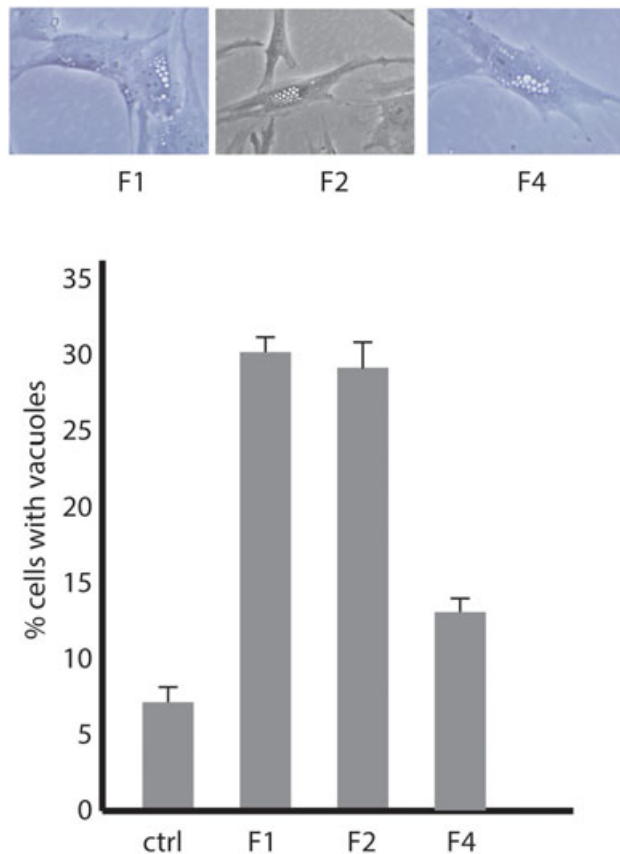


FIGURE 5 Patient fibroblasts from Family 1, Family 2 and Family 4 exhibit the characteristic vacuolization caused by deleterious variants of *FIG4*. (a) Live cell microscopy of cultured fibroblasts from affected individuals. (b) Quantitation of the extent of vacuolization. Values represent means ± SD, normal macula for comparison [Color figure can be viewed at wileyonlinelibrary.com]

together with the vacuolar phenotype suggests that Allele 1 is a partial loss-of-function allele (Figure 5).

4 | DISCUSSION

The leukodystrophies are defined as genetically determined disorders primarily affecting central nervous system white matter, irrespective of the structural white matter component involved, the molecular process affected, or the disease course (Kevelam et al., 2016). A classification of leukodystrophies grouping disorders according to cellular pathology has been proposed (Van der Knaap & Bugiani, 2017). In this classification *FIG4* leukodystrophy would be considered a myelin disorder, because *FIG4* has a direct role in oligodendrocyte maturation and Schwann cell myelination, in addition to its functions in neurons and other cells (Mironova et al., 2016; Vaccari et al., 2015).

The clinical consequences of partial loss-of-function variants of *FIG4* are highly heterogeneous, ranging from peripheral neuropathy in CMT4J to polymicrogyria with psychiatric components (Baulac et al., 2014; Nicholson et al., 2011). Comparison of the effects of

TABLE 1 Clinical description of affected individuals

Family ID	Family 1	Family 2	Family 3	Family 4	Family 5	Family 6	Family 7
Patient ID	Patient 1	Patient 2	Patient 3	Patient 4	Patient 5	Patient 6	Patient 7
Referrer	Vadlamani/ Livingston	Vadlamani/ Livingston	Stutterd	Stutterd	Tan	Tan	Tan
Sex	Male	Male	Male	Male	Male	Male	Female
Current age	4 years	11 years	11 years	4 years	11 years	8 years	6 years
Family history/ consanguinity/ ethnicity	No FH/ nonconsang/ white british		Anglo-Celtic		Anglo-Celtic		
Pregnancy complication	No	No	MRI evidence of prenatal ischaemic cerebral injury	No	No	No	No
Birth complication	No	No	Birth asphyxia	No	Previous first trimester miscarriages	No	No
Age of disease onset	5 months	Birth	<9 months	12 months	Neonatal period	Infancy	Infancy
Presenting symptom	Delayed motor development	Feeding difficulties and developmental delay	Hypotonia, developmental delay, and areflexia	Developmental delay	Feeding difficulties, global developmental delay, choreoathetoid movements, and bullseye maculopathy	Global developmental delay and bullseye maculopathy	Global developmental delay and bullseye maculopathy
Progressive disease	No	Yes	Yes	No	No	No	No
GMFCS/motor development at last review	GMFCS III	GMFCS V	GMFCS III	GMFCS II	GMFCS II	GMFCS II	GMFCS II
Movement disorder	No	No	Cerebellar ataxia	Mild tremor	Choreoathetoid movements	No	No
Other neurological complication, e.g., Seizure	No	No	No	No	No	No	No
Cognitive impairment	Few words, impaired understanding	Yes, moderate cognitive impairment	Low- borderline IQ	No speech at 4 year	Limited communication	Limited communication	Limited communication

(Continues)

TABLE 1 (Continued)

Family ID Patient ID	Family 1 Patient 1	Family 2 Patient 2	Family 3 Patient 3	Patient 4	Family 4 Patient 5	Patient 6	Patient 7
Vision impairment	No	No	Myopia, strabismus	Myopia, strabismus	No, but maculopathy	No, but maculopathy	No, but maculopathy
Other health problem or congenital disorder	No	Tracheostomy and gastrostomy	No		Feeding issues and vomiting in infancy	No	Explosive bowel movements streaked with blood in infancy, no pathology identified; self-resolved by 10 months
Nerve conduction study results	Not carried out	Prolonged latencies, very slow conduction velocity, and low CMAP	Mild-moderate demyelinating neuropathy	Mild-moderate demyelinating neuropathy; median n:22.8 m/s, tibial n:24.3 m/s	Not carried out	Not carried out	Not carried out
Age of MRIs (brain ± spine)	10 months and 27 months	30 months and 8 years.	12 months and 4 years	15 months	13 months, then 3 years	N/A	N/A
Pattern of white matter abnormality on MRI	Diffuse hypomyelination	T2 hyperintensity in deep cerebral white matter and posterior limb of internal capsule. Mild cerebellar atrophy	Periventricular T2 hypomyelination. Nerve roots enhancement suggestive of polyneuropathy.	Periventricular hypomyelination.	Ventricular dilatation detected at 13 months; reduction in white matter myelination at 3 years	N/A	N/A
Skeletal abnormality (clinically or radiologically)	No	No	Radiological finding: Thin shafts of the tubular bones with over tubulation, thin metacarpals, coxa valga, and dolichocephaly	Radiological findings: Delayed bone age, thin metacarpals, coxa valga, and dolichocephaly	No skeletal anomaly clinically	No skeletal anomaly clinically	No skeletal anomaly clinically
Chromosome position (Allele 1)	Chr6(GRCh37): g.110059618G > A	Chr6(GRCh37): g.110056361A > C	Chr6(GRCh37): g.110113868G > A	Chr6(GRCh37): g.110113868G > A	Chr6(GRCh37): g.110086256G > C	Chr6(GRCh37): g.110086256G > C	Chr6(GRCh37): g.110086256G > C

(Continues)

TABLE 1 (Continued)

Family ID Patient ID	Family 1 Patient 1	Family 2 Patient 2	Family 3 Patient 3	Family 4 Patient 4	Family 5 Patient 5	Family 6 Patient 6	Family 7 Patient 7
Chromosome position (Allele 2)	Chr6(GRCh37): g.110113868 G > A	Homozygous	Homozygous	Homozygous	Chr6(GRCh37): g.110113847_110-113849del	Chr6(GRCh37): g.110113847_110-113849del	Chr6(GRCh37): g.110113847_1101-13849del
cDNA variant (Allele 1)	NM_014845.5: c.737G > A	NM_014845.5 (FIG4):c.506A > C p.(Tyr169Ser)	2459 + 1G > A homozygous	2459 + 1G > A homozygous	NM_014845.5: c.1475G > C	NM_014845.5: c.1475G > C	NM_014845.5: c.1475G > C
cDNA variant (Allele 2)	NM_014845.5: c.2459 + 1G > A	(homozygous)	(homozygous)	(homozygous)	NM_014845.5: c.2439_2441del	NM_014845.5: c.2439_2441del	NM_014845.5: c.2439_2441del
Protein change (Allele 1)	p.Trp246Ter	p.Tyr169Ser	Truncation	Truncation	p.Arg492Pro	p.Arg492Pro	p.Arg492Pro
Protein change (Allele 2)	Truncation	Homozygous	Homozygous	Homozygous	p.Glu813del	p.Glu813del	p.Glu813del

Note. cDNA: complementary DNA; GMFCS: gross motor function classification system; MRI: magnetic resonance imaging

partial loss-of-function variants on enzymatic activity might help to clarify the distinction between the variants described in the present study and the variants seen in CMT4J, such as p.Ile41Thr (Nicholson et al., 2011). CNS hypomyelination is not a recognized feature of CMT4J.

The identification of four unrelated families with white matter defects and biallelic deleterious variants of *FIG4* confirms the important role of *FIG4* in myelinating glia. Our findings underline the importance of considering *FIG4* as a candidate gene in genomic studies of patients with myelination defects. Because of the variable phenotypes presented (skeletal features in one of the four families, macular features in one family, and variable degrees of CNS myelination across the cohort), phenotypic prioritization of *FIG4* in specific cases may be difficult, although peripheral neuropathy appears to be a common feature.

The exon 21 splice site variant was identified in a heterozygous state opposite a null allele in Family 1 and in a homozygous state in Family 3. The read-through transcript encodes a truncated protein containing 792 residues of the full-length protein (907 amino acids) plus 24 residues encoded by Intron 20. The truncated protein retains the protein interaction domain (Manford et al., 2010), and the catalytic active site (Guan & Dixon, 1991; Liu & Bankaitis, 2010) and has partial function. The missing 115 residues are poorly conserved through evolution and are absent from yeast *FIG4p*. In addition to the two families described here, this variant was previously identified in a patient with CMT disease; the other allele in this patient was not described (DiVincenzo et al., 2014).

The active-site mutation p.Arg492Pro in Family 4 was inherited in trans with a single amino acid deletion. The three affected siblings have a severe but nonlethal developmental disorder, indicating that one or both alleles retain partial function. We previously studied the active-site mutation p.Cys486Ser and found that expression of this mutant as a transgene extended the survival of *FIG4* null mice (Lenk et al., 2016a). These two active-site mutants indicate that the *FIG4* protein also has a nonenzymatic function such as stabilization of the PI(3,5)P2 biosynthetic complex in vivo. The presence of maculopathy in all three siblings suggests that this is part of their syndrome, but further work will be required to exclude another cause. There has been one report of a macular phenotype in Yunis-Varon syndrome (Corona-Rivera et al., 2011), suggesting that children with *FIG4*-associated CNS myelination defects should undergo ocular examinations.

The affected individuals in Family 3 have skeletal abnormalities that overlap with Yunis-Varón syndrome. Patient 3 has progressive scoliosis requiring surgical management. Systemic x-rays demonstrate thin shafts in the tubular bones and over tubulation, a feature also seen in Yunis-Varón syndrome. His younger brother had no clinical evidence of skeletal disease but his x-rays demonstrate delayed bone age. Both siblings also exhibit thin metacarpals, coxa valga, and dolichocephaly. These subtle skeletal abnormalities support the view that hypomyelination and Yunis-Varón syndrome are representative of a spectrum of *FIG4* deficiency disease.

The role of FIG4 in oligodendrocyte maturation was previously studied in FIG4 null mice. Primary oligodendrocytes in culture develop enlarged LAMP1-positive vesicles that accumulate myelin-associated glycoprotein and fail to migrate to the nascent myelin sheet, demonstrating the dependence of myelin biosynthesis on FIG4 function (Mironova et al., 2016). In addition, induced knockout of FIG4 in the adult mouse prevents repair of a chemically-induced white matter lesion (Mironova et al., 2018). These findings provide a cellular mechanism to explain the effects of pathogenic variants of FIG4 on CNS white matter. The observed heterozygosity for a deleterious allele in an individual with multiple sclerosis reported here may be an incidental finding, but the role of FIG4 in myelination suggests that follow-up studies would be worthwhile.

In summary, we identified four families with novel FIG4 genotypes and CNS white matter disease varying from severe hypomyelination to mild undermyelination, in addition to peripheral neuropathy. Impaired FIG4 function was revealed by the presence of large vacuoles in cultured patient fibroblasts. Abnormal messenger RNA splicing and nonsense-mediated decay were characterized in two families. Inheritance of unique combinations of variants with partial loss-of-function of FIG4 results in disease severity that lies between the lethal Yunis-Varón syndrome and the milder CMT4J. The clinical management of patients with pathogenic variants in FIG4 should include assessment of peripheral neuropathy, CNS hypomyelination, and skeletal disease. The prominent CNS white matter defects in three of these four families indicate that FIG4 should be considered a candidate gene in individuals presenting with leukoencephalopathy.

ACKNOWLEDGMENTS

The authors thank the patients and their families for participating in this study. We thank James Tellez, Northern Genetics Service, Institute of Genetic Medicine, Centre for Life, Newcastle upon Tyne, for RNA analysis of Family 1 that was not included in this study. Funding to M.H.M. and G.M.L. was provided by NIGMS (R01 GM24872). Sequencing of Family 4 was carried out by the Center for Mendelian Genomics at the Broad Institute of MIT and Harvard and was funded by the National Human Genome Research Institute, the National Eye Institute, and the National Heart, Lung and Blood Institute grant UM1 HG008900 to Daniel MacArthur and Heidi Rehm. CAS was supported by NHMRC Postgraduate Scholarship (GNT1133266) and the Royal Children's Hospital/Murdoch Childrens Research Institute Flora Suttie Neurogenetics Fellowship made possible by the Thyne-Reid Foundation and the Macquarie Foundation. Additional funding was provided by the NHMRC Independent Research Institute Infrastructure Support Scheme and the Victorian State Government Operational Infrastructure Program. Conception and design of the study was completed by M.H.M. and G.M.L., acquisition and analysis of data were performed by M.H.M., G.M.L., I.R.B., C.A.S., C.S., A.V., V.R.C., M.F.F., O.S., P.L., R.L., T.Y.T., S.G., S.M.W., J.C.G.M.L., I.R.B., C.A.S., and T.Y.T. Drafting a significant portion of the manuscript or figures were completed by M.H.M., G.M.L., J.H.L., and C.A.S.

ORCID

Guy M. Lenk  <http://orcid.org/0000-0001-8092-1405>

REFERENCES

- Baulac, S., Lenk, G. M., Dufresnois, B., Ouled Amar Bencheikh, B., Couarch, P., Renard, J., ... Leguern, E. (2014). Role of the phosphoinositide phosphatase FIG4 gene in familial epilepsy with polymicrogyria. *Neurology*, 82, 1068–1075.
- Campeau, P. M., Lenk, G. M., Lu, J. T., Bae, Y., Burrage, L., Turnpenny, P., ... Lee, B. H. (2013). Yunis-Varon syndrome is caused by mutations in FIG4, encoding a phosphoinositide phosphatase. *American Journal of Human Genetics*, 92, 781–791.
- Chow, C. Y., Zhang, Y., Dowling, J. J., Jin, N., Adamska, M., Shiga, K., ... Meisler, M. H. (2007). Mutation of FIG4 causes neurodegeneration in the pale tremor mouse and patients with CMT4. *Nature*, 448, 68–72.
- Cingolani P, Platts A, Wang le L, Coon M, Nguyen T, Wang L, Ruden D.M. A program for annotating and predicting the effects of single nucleotide polymorphisms, SnpEff: SNPs in the genome of *Drosophila melanogaster* strain w1118; iso-2; iso-3 *Fly (Austin)* 2 6 2012.80-92 <https://doi.org/10.4161/fly.19695>
- Corona-Rivera, J. R., Romo-Huerta, C. O., López-Marure, E., Ramos, F. J., Estrada-Padilla, S. A., & Zepeda-Romero, L. C. (2011) New ocular findings in two sisters with Yunis-Varón syndrome and literature review. *European Journal of Medical Genetics*, 54, 76–81.
- DiVincenzo, C., Elzinga, C. D., Medeiros, A. C., Karbassi, I., Jones, J. R., Evans, M. C., ... Higgins, J. J. (2014). The allelic spectrum of Charcot-Marie-Tooth disease in over 17,000 individuals with neuropathy. *Molecular Genetics & Genomic Medicine*, 2, 522–529.
- Dong, X., Shen, D., Wang, X., Dawson, T., Li, X., Zhang, Q., ... and Xu, H. (2010). controls membrane trafficking by direct activation of mucopolip Ca(2+) release channels in the endolysosome. *Nature Communications*, 13, 1–38.
- Ferguson, C. J., Lenk, G. M., Jones, J. M., Grant, A. E., Winters, J. J., Dowling, J. J., ... Meisler, M. H. (2012). Neuronal expression of Fig4 is both necessary and sufficient to prevent spongiform neurodegeneration. *Human Molecular Genetics*, 21, 3525–3534.
- Ferguson, C. J., Lenk, G. M., & Meisler, M. H. (2009). Defective autophagy in neurons and astrocytes from mice deficient in PI(3,5)P2. *Human Molecular Genetics*, 18, 4868–4878.
- Guan, K., Dixon, J. E. (1991). Eukaryotic proteins expressed in *Escherichia coli*: An improved thrombin cleavage and purification procedure of fusion proteins with glutathione S-transferase. *Anal of Biochemistry*, 192, 262–267.
- Jin, N., Chow, C. Y., Liu, L., Zolov, S. N., Bronson, R., Davisson, M., ... Weisman, L. S. (2008). VAC14 nucleates a protein complex essential for the acute interconversion of PI3P and PI(3,5)P(2) in yeast and mouse. *The EMBO Journal*, 27, 3221–3234.
- Kevelam, S., Steenweg, M., Srivastava, S., Helman, G., Naidu, S., Schiffmann, R., ... van der Knaap, M. (2016). Update on leukodystrophies: A historical perspective and adapted definition. *Neuropediatrics*, 47(6), 349–354.
- Kirsch S. A., Kugemann A., Carpaneto A., Böckmann R. A., Dietrich P. (2018). Phosphatidylinositol-3,5-bisphosphate lipid-binding-induced activation of the human two-pore channel 2 *Cellular and Molecular Life Science*, 75(20), 3803–3815 .
- Van der Knaap, M. S., & Bugiani, M. (2017). Leukodystrophies: A proposed classification system based on pathological changes and pathogenetic mechanisms. *Acta Neuropathologica*, 134 (3), 35–382.
- Lek, M., Karczewski, K. J., Minikel, E. V., Samocha, K. E., Banks, E., Fennell, T., ... MacArthur, D. G. (2016) Analysis of protein-coding genetic variation in 60, 706 humans. *Nature*, 536, 285–291.

- Lenk, G. M., Ferguson, C. J., Chow, C. Y., Jin, N., Jones, J. M., Grant, A. E., ... Meisler, M. H. (2011). Pathogenic mechanism of the FIG4 mutation responsible for Charcot-Marie-Tooth disease CMT4J. *PLOS Genetics*, 7, e1002104.
- Lenk, G. M., Frei, C. M., Miller, A. C., Wallen, R. C., Mironova, Y. A., Giger, R. J., ... Meisler, M. H. (2016a) Rescue of neurodegeneration in the Fig4 null mouse by a catalytically inactive FIG4 transgene. *Human Molecular Genetics*, 25, 340–347.
- Lenk, G. M., & Meisler, M. H. (2014). Mouse models of PI(3,5)P2 deficiency with impaired lysosome function. *Methods in Enzymology*, 534, 245–260. <https://doi.org/10.1016/B978-0-12-397926-1.00014-7>
- Lenk, G. M., Szymanska, K., Debska-Vielhaber, G., Rydzanicz, M., Walczak, A., Bekiesinska-Figatowska, M., ... Ploski, R. (2016b). Biallelic mutations of VAC14 in pediatric-onset neurological disease. *American Journal of Human Genetics*, 99, 188–194.
- Li, H., Durbin, R. (2009). Fast and accurate short read alignment with Burrows-Wheeler transform *Bioinformatics* 25, 1754–1760.
- Liu, Y., Bankaitis, V. A. (2010). Phosphoinositide phosphatases in cell biology and disease *Progress in Lipid Research*, 49, 201–217.
- Manford, A., Xia, T., Saxena, A. K., Stefan, C., Hu, F., Emr, F., Mao, Y. (2010). Crystal structure of the yeast Sac1: implications for its phosphoinositide phosphatase function *EMBO Journal*, 29, 1489–1498.
- McKenna, A., Hanna, M., Banks, E., Sivachenko, A., Cibulskis, K., Kernytsky, A., DePristo, M. A. (2010). The Genome Analysis Toolkit: a MapReduce framework for analyzing next-generation DNA sequencing data *Genome Research*, 9, 20, 1297–1303. <https://doi.org/10.1101/gr.107524.110>
- Mironova, Y. A., Lenk, G. M., Lin, J. P., Lee, S. J., Twiss, J. L., Vaccari, I., ... Giger, R. J. (2016). PI(3,5)P2 biosynthesis regulates oligodendrocyte differentiation by intrinsic and extrinsic mechanisms. *eLife*, 5, e13023.
- McDonald, J. M., Krainc, D. (2017). Lysosomal Proteins as a Therapeutic Target in Neurodegeneration *Annual Review of Medicine*, 1, 68, 445–458. <https://doi.org/10.1146/annurev-med-050715-104432>
- Mironova, Y. A., Lin, J.-P., Kalinski, A., Huffman, L., Lenk, G. M., Havton, L. A., ... Giger, R. J. (2018) Protective role of the lipid phosphatase Fig4 in the adult nervous system. *Human Molecular Genetics*, 27, 2443–2453.
- Nicholson, G., Lenk, G. M., Reddel, S. W., Grant, A. E., Towne, C. F., Ferguson, C. J., ... Meisler, M. H. (2011). Distinctive genetic and clinical features of CMT4J: A severe neuropathy caused by mutations in the PI(3,5)P(2) phosphatase FIG4. *Brain*, 134, 1959–1971.
- Polman, C. H., Reingold, S. C., Banwell, B., Clanet, M., Cohen, J. A., Filippi, M., ... Wolinsky, J. S. (2011) Diagnostic criteria for multiple sclerosis. *Annals of Neurology*, 69, 292–302.
- She, J., Guo, J., Chen, Q., Zeng, W., Jiang, Y., Bai, X. (2018) Structural insights into the voltage and phospholipid activation of the mammalian TPC1 channel. *Nature*, 556, 130–134.
- Stutterd, C., Diakumis, P., Bahlo, M., Fanjul Fernandez, M., Leventer, R. J., Delatycki, M., ... Lockhart, P. J. (2017). Neuropathology of childhood-onset basal ganglia degeneration caused by mutation of VAC14. *Annals of Clinical and Translational Neurology*, 4(12), 859–864.
- Vaccari, I., Carbone, A., Previtali, S. C., Mironova, Y. A., Alberizzi, V., Nosedà, R., ... Bolino, A. (2015). Loss of Fig4 in both Schwann cells and motor neurons contributes to CMT4J neuropathy. *Human Molecular Genetics*, 24, 383–396.
- Wang, X., Zhang, X., Dong, X., Samie, M., Li, X., Cheng, X., ... and Xu, H. (2012). TPC proteins are phosphoinositide-activated sodium-selective ion channels in endosomes and lysosomes. *Cell*, 12, 372–383.
- Wilson, Z. N., Scott, A. L., Dowell, R. D., Odorizzi, G. (2018) PI(3,5)P(2) controls vacuole potassium transport to support cellular osmoregulation. *Molecular Biology of the Cell*, 29, 1718–1731.
- Winters, J. J., Ferguson, C. J., Lenk, G. M., Giger-Mateeva, V. I., Shrager, P., Meisler, M. H., & Giger, R. J. (2011). Congenital CNS hypomyelination in the Fig4 null mouse is rescued by neuronal expression of the PI(3,5)P(2) phosphatase Fig4. *The Journal of neuroscience*, 31, 17736–17751.
- Zolov, S. N., Bridges, D., Zhang, Y., Lee, W. W., Riehle, E., Verma, R., ... Weisman, L. S. (2012). In vivo, Pikfyve generates PI(3,5)P2, which serves as both a signaling lipid and the major precursor for PI5P. *Proceedings of the National Academy of Sciences of the United States of America*, 23, 17472–17477.

SUPPORTING INFORMATION

Additional supporting information may be found online in the Supporting Information section at the end of the article.

How to cite this article: Lenk GM, Berry IR, Stutterd CA, et al. Cerebral hypomyelination associated with biallelic variants of FIG4. *Human Mutation*. 2019;40:619–630. <https://doi.org/10.1002/humu.23720>